

Article

## Glucose Sensing by Time-Resolved Fluorescence of Sol-Gel Immobilized Glucose Oxidase

Rosario Esposito <sup>1,\*</sup>, Bartolomeo Della Ventura <sup>2</sup>, Sergio De Nicola <sup>3</sup>, Carlo Altucci <sup>1</sup>,  
Raffaele Velotta <sup>1</sup>, Damiano Gustavo Mita <sup>2,4</sup> and Maria Lepore <sup>2</sup>

<sup>1</sup> CNISM-Dipartimento Scienze Fisiche, Università di Napoli Federico II, Napoli 80126, Italy;  
E-Mails: altucci@na.infn.it (C.A.); velotta@na.infn.it (R.V.)

<sup>2</sup> Dipartimento di Medicina Sperimentale, Seconda Università di Napoli, Napoli 80138, Italy;  
E-Mails: dellaventura@na.infn.it (B.D.V.); mita@igb.cnr.it (D.G.M.); maria.lepore@unina2.it (M.L.)

<sup>3</sup> Istituto Nazionale di Ottica, CNR, compr. A. Olivetti, Via Campi Flegrei 34, Pozzuoli 80078, Italy;  
E-Mail: s.denicola@cib.na.cnr.it

<sup>4</sup> Institute of Genetics and Biophysics, CNR, Naples 80131, Italy

\* Author to whom correspondence should be addressed; E-Mail: rosesp@na.infn.it;  
Tel.: +39-081-676-293; Fax: +39-081-676-346.

Received: 11 February 2011; in revised form: 14 March 2011 / Accepted: 16 March 2011 /

Published: 24 March 2011

---

**Abstract:** A monolithic silica gel matrix with entrapped glucose oxidase (*GOD*) was constructed as a bioactive element in an optical biosensor for glucose determination. Intrinsic fluorescence of free and immobilised *GOD* was investigated in the visible range in presence of different glucose concentrations by time-resolved spectroscopy with time-correlated single-photon counting detector. A three-exponential model was used for analysing the fluorescence transients. Fractional intensities and mean lifetime were shown to be sensitive to the enzymatic reaction and were used for obtaining calibration curve for glucose concentration determination. The sensing system proposed achieved high resolution (up to 0.17 mM) glucose determination with a detection range from 0.4 mM to 5 mM.

**Keywords:** glucose oxidase; biosensors; glucose determination; time-resolved fluorescence; lifetime

**Classification:** PACS 87.85.fk; 87.64.kv; 78.47.D-; 33.70.Ca

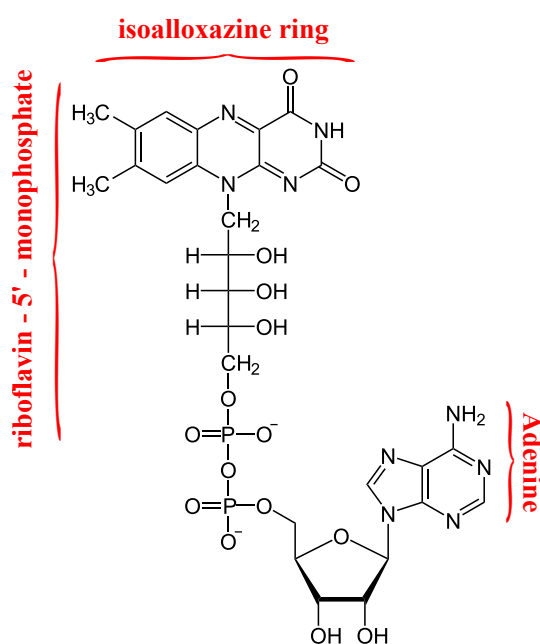
---

## 1. Introduction

In the last years the employment of glucose oxidase (*GOD*) in glucose optical sensing has been largely investigated for clinical and industrial applications [1–8]. Different immobilization procedures have been adopted [9–11] aiming to improve the linear range, sensibility, specificity, reproducibility and time stability of the optical sensors. Sol-gel matrices have been proven to be excellent carriers for enzymes since their catalytic activity is slightly affected by the gel structure. In addition sol-gel avoids the leakage of the bioactive macromolecule and allows the diffusion of substrate (and reaction products) towards (or away from) the catalytic site [12–14].

It is well known that *GOD* is a homo-dimer composed of two identical 80-kDa subunits and two non-covalently bound flavin adenine dinucleotides complexes (*FAD*). *FAD* is situated in the first domain which consists of two beta sheets and three alpha helices and occupies a narrow channel outlined by 31 residues with a covering lid formed by residues 75–98 [15]. The *FAD* structure is composed by flavoprotein and adenine dinucleotide (Figure 1). The isoalloxazine (*ISO*) ring is responsible for the light emission of *FAD* in the visible spectral range and is linked with adenine through hydrogen-bonding. It was proposed that *FAD* exists in two conformations: an extended, open conformation, and a closed one, in which the isoalloxazine and adenine rings interact through a stacked conformation. The open conformation gives rise to the fluorescent component of *FAD* with lifetime  $\sim 2.8$  ns, whereas a much faster fluorescence decay ( $\sim 4$  ps) takes place as a consequence of the photoinduced electron transfer (ET) between adenine and flavin [16,17]. The conformational changes experienced by the molecule during the lifetime of the excited states accounts for an intermediate lifetime component of  $\sim 0.3$  ns.

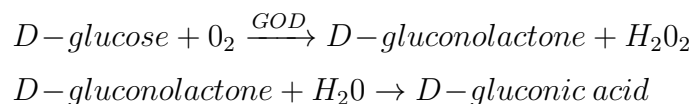
**Figure 1.** Structural formula of flavin adenine dinucleotide (*FAD*).



In flavins, photoinduced ET from adenine to excited *ISO* competes with the reductive ET mechanism that involves tyrosine and tryptophan residues adjacent to *ISO*. Particularly, X-ray crystallographic structure of *GOD* showed that four aromatic residues, Tyr515, Trp426, Tyr68, and Trp111, are in close contact with the isoalloxazine moiety of *FAD* and these residues serve as electron donors in the

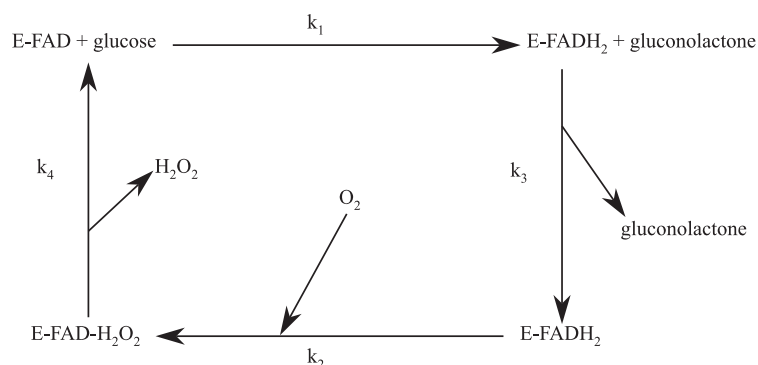
photoinduced reductive ET [18,19]. With femtosecond resolution, the fluorescence quenching of *GOD* due to ET with aromatic residues has been investigated and two decay constants of 1.8 ps and 10 ps have been measured [20]. Thus, we can assume three ranges for fluorescence lifetimes in flavins: long ( $\sim 2.0\text{--}3.0$  ns), intermediate ( $\sim 300$  ps) and short ( $\leq 10$  ps).

Dynamical changes of *FAD* fluorescence are exhibited when oxidative processes are induced in *GOD* by means of glucose interaction [21–23]. In fact, *GOD* catalyses the oxidation of glucose to gluconic acid through the reaction:



The well-known reaction mechanism is the following: glucose reduces *FAD* to *FADH*<sub>2</sub> with formation of gluconolactone, which is rapidly hydrolysed to gluconic acid. At this point the dissolved oxygen reoxidises *FADH*<sub>2</sub> and produces *H*<sub>2</sub>*O*<sub>2</sub>. According to the cyclic scheme of Figure 2, two species display the fluorescence of *FAD* and *FADH*<sub>2</sub>.

**Figure 2.** Scheme of the enzymatic reaction. *O*<sub>2</sub> is the oxygen concentration in the bulk solution.



The chemical reduction of *FAD* to *FADH*<sub>2</sub> should affect the reductive photoinduced ET interaction with the surrounding aromatic residues. The glucose and oxygen concentrations and the induced change of the pH environment could contribute to alter the usual equilibrium between the normal and closed conformations of *FAD*, thus causing a change in the fluorescence intensity [24]. In Reference [25] some of us have investigated on the possibility of using that change in *GOD* immobilised in a silica gel matrix for glucose based biosensor. To this regard, physicochemical and biochemical characterizations of the catalytic matrix have been performed and the intrinsic fluorescence of immobilised *GOD* has been investigated by steady-state fluorescence measurements. The silica gel matrix has been proved to be a suitable support for optical biosensing owing to its superior optical properties such as high transmittance, reproducibility of *GOD* fluorescence and absorption spectra after immobilization. Moreover, calibration curves as a function of glucose concentration have been obtained by steady-state measurements with sensitivity and linear calibration range comparable to the other immobilization systems.

However, it has been shown [26] that the use of decay times, as opposed to intensities, is preferred in view of their independence on probe concentrations as well as the intensity fluctuations of the fluorescence signal. Moreover, lifetimes can be measured also in highly scattering media [27,28]. In

fact, successful measurements through several layers of chicken skin have been performed, giving a promising issue for glucose sensing in real samples like tissue and blood [29].

In this paper we investigate the dynamic behaviour of interactions between free *GOD* and glucose and the modifications occurring when *GOD* is immobilized in the silica gel matrix used in Reference [25]. We use time-resolved fluorescence for accurate measurements of fractional intensities and lifetimes as sensitive parameters to the enzymatic reaction of *GOD* with glucose and we show that it is possible to achieve improvements of the performances of the sensing system.

The outline of the paper is the following. In Section 2 we describe the materials and methods adopted to realize sol-gel matrices that immobilize *GOD*. Experimental setup used for steady-state and time-resolved measurements are also reported together with the multi-exponential model adopted to analyse decay curves. Steady state and time-resolved fluorescence measurements for free *GOD* without and with glucose are discussed in Section 3.1, and experimental results for immobilised *GOD* are analysed in Section 3.2. Moreover, steady-state and temporal profiles for free and immobilised cases are compared. In Section 3.3 the fractional intensities of lifetime components are retrieved by means of a fitting procedure and their behaviour are analysed for obtaining calibration curves as a function of glucose concentration. To conclude, the analytical performance of the proposed sensing system is compared with that of various *GOD* based optical biosensors in terms of the immobilization support, detection method, stability, linear range and detection limits.

## 2. Materials and Methods

### 2.1. Materials

All chemicals were purchased from Sigma (Sigma Italia, Milan, Italy), with the exception of tetramethoxysilane (TMOS) and glucose oxidase (*GOD*), which were purchased from Fluka (Fluka Italia, Milan, Italy). In this study glucose oxidase (*GOD*, EC 1.1.3.4) from *Aspergillus niger* ( $154 \text{ U mg}^{-1}$ ) was used.

### 2.2. Methods

#### 2.2.1. Preparation of the Catalytic Sol-Gel Matrices

Silica gel matrices were prepared, as described in a previous paper [9], by rapid mixing  $800 \mu\text{L}$  of solution A with  $800 \mu\text{L}$  of solution B in a polymethylmethacrylate cell. Solution A was obtained by slowly mixing (for 1 h at  $4 \text{ }^\circ\text{C}$ ) TMOS ( $1,550 \mu\text{L}$ ) with  $\text{H}_2\text{O}$  ( $450 \mu\text{L}$ ) plus  $40 \text{ mM}$  HCl ( $30 \mu\text{L}$ ). Solution B contained  $0.1 \text{ M}$  phosphate buffer at pH 6.5. The A and B solution mixture ( $1,600 \mu\text{L}$ ) was poured into a polymethylmethacrylate cell that was sealed with paraffin film and placed horizontally until the gel was formed. To avoid cracking in the formed gel, the cell was filled with  $0.1 \text{ M}$  phosphate buffer at pH 6.5 and stored overnight in a refrigerator at  $4 \text{ }^\circ\text{C}$ . The day after, the silica gel layer was removed from the cell and was ready for use. The catalytic gel was obtained with solution B containing an additional  $20 \text{ mg/mL}$  of *GOD* in  $0.1 \text{ M}$  phosphate buffer at pH 6.5.

Generally, the retention of *GOD* activity after entrapment in silica gel is very low since the entrapment of *GOD* changes the properties of the enzyme, especially its stability [30]. The change in the properties

of the enzyme inside the gel is due to the change in its conformation leading sometimes to a denaturation of protein, restriction of molecule motion and lower accessibility of the entrapped enzyme by the substrate [14]. The changes of protein conformation and dynamic motion inside the gel are caused by interactions of the molecule with silica surface inside the pores and different micro-environment. As a result, the activity of the entrapped enzyme is typically lower and the stability can either be decreased or increased depending on the composition of the gel [14]. The properties of *GOD* immobilised in the proposed silica gel have been extensively investigated in Reference [25]. It results an apparent value of Michaelis–Menten constant larger than that obtained for free *GOD* as a result of its lower activity. Moreover, the investigations have evidenced a high catalytic stability of the gel since only a decrease of about 2% for the absorbance spectrum has been observed after 60 days. In the following all the measurements have been performed at room temperature.

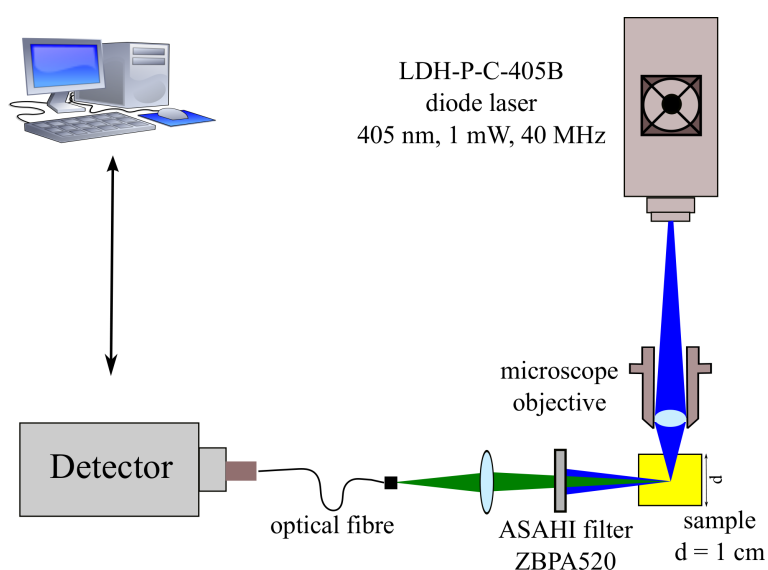
### 2.2.2. Steady-State Fluorescence Measurements

The emission fluorescence spectra have been collected by means of a spectrofluorimeter (model LS 55, Perkin-Elmer), by using as light source a Xenon discharge lamp with an emission spectrum ranging from 200 to 800 nm. Sample excitation was performed at 450 nm, while the emission spectrum was recorded in the range 480–580 nm. The spectra have been acquired with entrance and exit slit fixed at 5 nm and with a scan speed of 100 nm s<sup>-1</sup>.

### 2.2.3. Time-Resolved Fluorescence Measurements

Time-resolved fluorescence experiments were carried out using the experimental setup shown in Figure 3.

**Figure 3.** Experimental setup.



Excitation for the solution was provided by a picosecond diode laser (Picoquant, LDH-P-C-405B) emitting pulses at repetition rate of 40 MHz and a wavelength of 405 nm, close to the absorption maximum of the first electronic transition of the bound flavin. The laser beam was focused into a

10 mm sample cell by a simple microscope objective lens. The fluorescence light was detected at 90° to the incident light beam to minimize the amount of transmitted or reflected beam light reaching the detector. An Asahi ZBPA520 bandpass filter blocks the residual laser beam and allows only radiation with a wavelength of  $520 \pm 10$  nm to reach the detector, that is a wavelength range close to the maximum of fluorescence emission spectrum of *GOD*. The detection apparatus was composed of a fast multichannel plate photomultiplier tube (MCP-PMT) (R4110U-05-F008aA, Hamamatsu, Tokyo, Japan) and a time-correlated single-photon counting (TCSPC) electronics (SPC300, Becker and Hickl GmbH, Berlin, Germany). The instrument response function (IRF) determined by TCSPS was about 120 ps FWHM.

Analysis of fluorescence transients was performed through a fitting procedure with a three-exponential model, in agreement with the description of redox reaction proposed in References [16,20]. Effects of the system response have been taken into account by convolving the analytical model with IRF, according to the following expression:

$$I(t) = IRF(t) \otimes \sum_{i=1}^3 \frac{\alpha_i}{\tau_i} \exp\left(-\frac{t}{\tau_i}\right) \quad (1)$$

where the pre-exponential factor  $\alpha_i$  is the total fluorescence intensity for the  $i^{th}$  emitting component with lifetime  $\tau_i$ . The mean lifetime  $\bar{\tau}$  is obtained by the classical relationship:

$$\bar{\tau} = \frac{\sum \alpha_i \tau_i}{\sum \alpha_i} = \sum f_i \tau_i, \quad (2)$$

where  $f_i$  are the fractional steady-state intensities of each lifetime component:

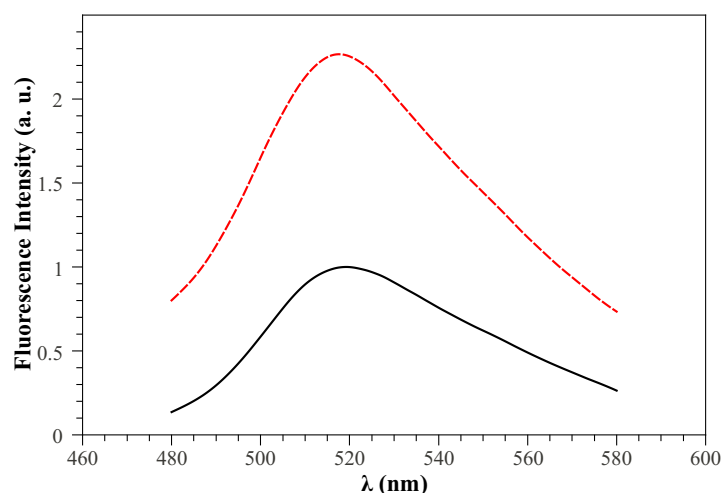
$$f_i = \frac{\alpha_i}{\sum \alpha_i} \quad (3)$$

### 3. Results and Discussion

#### 3.1. Free *GOD*

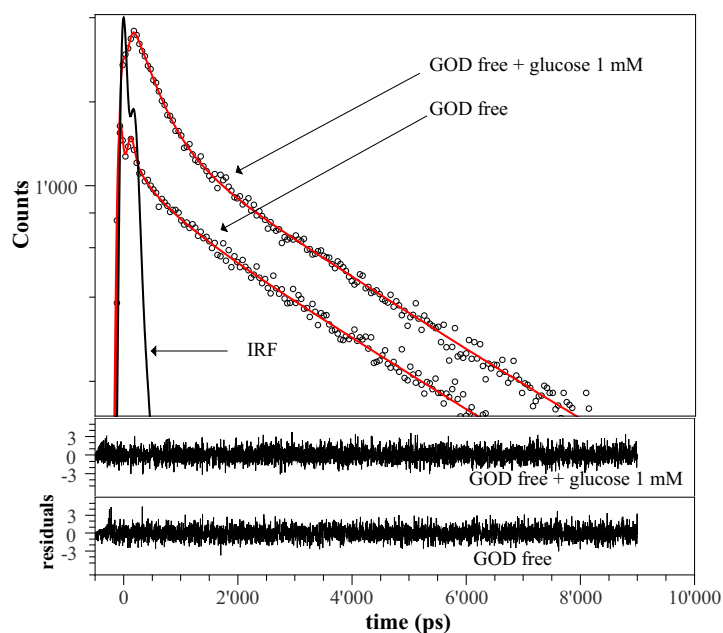
As a preliminary step we examined the steady-state fluorescence properties of free *GOD* and the changes induced by glucose addition. According to the results reported in Reference [31], the maximum of the fluorescence emission of free *GOD* was at 520 nm when the excitation is at 450 nm. Generally, the effect of glucose addition is to increase the peak value and the area of the fluorescence intensity emission spectrum, since reduced and oxidized flavins (*FADH<sub>2</sub>* and *FAD*) exhibit different fluorescent properties [24]. Figure 4 shows, as an example, the fluorescence emission spectra of soluble *GOD* in absence (black solid curve) and in the presence of 1 mM glucose concentration (red dotted curve). It can be clearly seen that the inclusion of glucose results in a fluorescence peak value that almost doubles with a corresponding increase of the integral area under the spectrum.

**Figure 4.** Free *GOD* fluorescence emission spectrum in the *FAD* region ( $\lambda_{exc} = 450 \text{ nm}$ ) without (black solid curve) and with (red dotted curve) 1 *mM* glucose concentration.



A better understanding of the fluorescence intensity enhancement is given by time-resolved measurements. To this regard, we have plotted in Figure 5 the decays curves (black points) for *GOD* in absence and in presence of 1 *mM* glucose concentration. The random distribution of residuals around zero confirms that the observed data can be satisfactorily fitted with the three-exponential model (1) (red solid curves). The estimated parameters are shown in Table 1 and their values are in quite good agreement with results reported in References [16,20] for free *GOD*.

**Figure 5.** Black points represents the fluorescence decays for free *GOD* when excited in the *FAD* region ( $\lambda_{exc} = 405 \text{ nm}$ ) without and with glucose (1 *mM*). Red solid curves are three-exponential fits. The instrument response function is shown for comparison with the fluorescence decay. In the lower panels residuals for three-exponential models are reported. The fitting parameters are shown in Table 1.



The sum of fluorescence intensities,  $\sum_{i=1}^3 \alpha_i$ , is comparable with intensities of steady-state measurements and increases to about 87% upon glucose addition. In particular, the values of fractional intensities  $f_i$  reported in Table 1 are clear evidence of a fluorescence quenching of the fast and long component  $\tau_1$  and  $\tau_3$ . The intensities  $f_1$  and  $f_3$  change from 0.054 to 0.015 and from 0.88 to 0.76, respectively. Conversely, the intermediate fluorescence component  $f_2$  increases from 0.06 to 0.22 accounting for the overall enhancement of the fluorescence intensity as glucose is added into the aqueous solution.

**Table 1.** Amplitude  $\alpha_i$ , total fluorescence intensity  $\sum_{i=1}^3 \alpha_i$ , lifetime  $\tau_i$ , mean lifetime  $\bar{\tau}$ , and relative amplitude  $f_i$  of the three-exponential model for free and immobilized *GOD* in absence and in presence of glucose.

|                   | <i>GOD</i> free | <i>GOD</i> free<br>+ 1 mM glucose | <i>GOD</i><br>immobilized | <i>GOD</i><br>immobilized<br>+ 2 mM glucose |
|-------------------|-----------------|-----------------------------------|---------------------------|---|
| $\alpha_1$        | 0.031 ± 0.004   | 0.02 ± 0.01                       | 0.08 ± 0.01               | 0.037 ± 0.006                               |
| $\alpha_2$        | 0.035 ± 0.004   | 0.230 ± 0.003                     | 0.094 ± 0.01              | 0.476 ± 0.006                               |
| $\alpha_3$        | 0.490 ± 0.003   | 0.790 ± 0.003                     | 0.4 ± 0.01                | 0.643 ± 0.005                               |
| $\sum \alpha_i$   | 0.556           | 1.04                              | 0.574                     | 1.156                                       |
| $\tau_1$ (ps)     | 3 ± 1           | 2 ± 1                             | 8 ± 3                     | 4 ± 2                                       |
| $\tau_2$ (ps)     | 550 ± 60        | 401 ± 8                           | 380 ± 70                  | 450 ± 7                                     |
| $\tau_3$ (ps)     | 3,120 ± 40      | 3,061 ± 28                        | 2,960 ± 190               | 3,010 ± 50                                  |
| $\bar{\tau}$ (ps) | 2,784           | 2,413                             | 2,126                     | 1,860                                       |
| $f_1$             | 0.054           | 0.015                             | 0.14                      | 0.029                                       |
| $f_2$             | 0.06            | 0.22                              | 0.16                      | 0.41  |
| $f_3$             | 0.88            | 0.76                              | 0.70                      | 0.56  |

### 3.2. Immobilized *GOD*

The black curve of Figure 6 represents the fluorescence spectrum of *GOD* immobilized in a sol gel layer. Also in this case, the presence of glucose in solution has the effect of enhancing the fluorescence intensity as it is evidenced by the red curve shown in Figure 6 where a 2 mM glucose concentration has been considered. Both peaks and integral area under the spectrum increase by about 36%.

In Figure 7 the theoretical model of Equation (1) (red curves) has been fitted with the fluorescence decay curves (black points) measured in the same experimental conditions of Figure 6.

The results of fitting are reported Table 1 showing that the immobilization matrix affects the relative contribution  $f_i$  of the three fluorescent components. In particular, the first two components,  $\tau_1$  and  $\tau_2$ , increase their fractional intensity to the detriment of the long fluorescence lifetime component  $\tau_3$ . It is worth noticing that the inclusion of glucose leads to the same qualitative effects observed in free *GOD*, i.e., (i) an increase of the total fluorescence intensity, and (ii) a quenching of the fast and slow fluorescence components to the benefit of the intermediate one.

**Figure 6.** Immobilized *GOD* fluorescence emission spectrum in the FAD region ( $\lambda_{exc} = 405$  nm) without (black curve) and with (red curve) 2 mM glucose concentration.

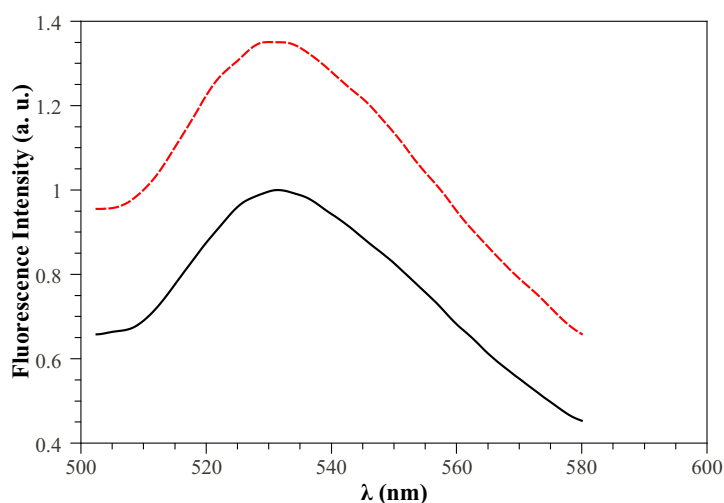
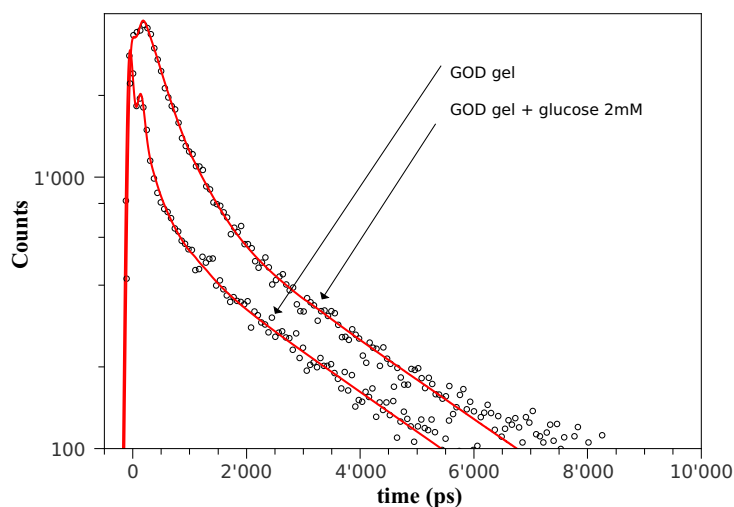


**Figure 7.** Black points are the fluorescence decays for immobilized *GOD* when excited in the FAD region ( $\lambda_{exc} = 405$  nm) without and with glucose (2 mM). Red curves are three-exponential fits. The fitting parameters are reported in Table 1.

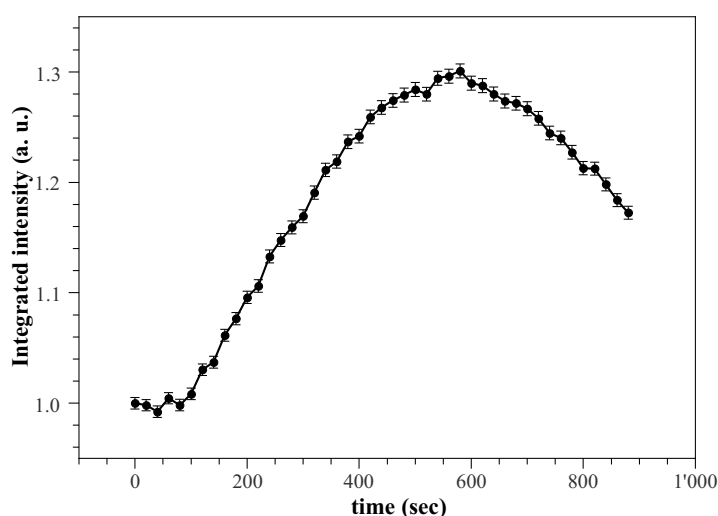


Actually, the fluorescence enhancement lasts until the reaction cycle of Figure 2 takes place. To this regard, changes in fluorescence decay caused by the enzymatic reaction upon the addition of 2 mM glucose concentration, were monitored every 20 s with acquisition time of 20 s. The integral area of decay curves have been normalized to the value observed before the enzymatic reaction starts. Figure 8 shows the normalized data as a function of reaction time. The total fluorescence intensity initially remains constants and after some time it increases gradually to a maximum value of about 30% greater than that obtained in free *GOD* condition. Then, the fluorescence intensity tends to decrease gradually. Similar behaviour has been observed at any glucose concentration and has been extensively discussed in Reference [21]. This behaviour has been ascribed to the kinetics of the process, in particular to the reoxidation of  $FADH_2$ . The reoxidation process proceeds at a constant rate greater than that at which the solution takes up  $O_2$  from the surrounding atmosphere (mass transfer). Initially, the reaction

involves a net uptake of  $O_2$ , since the mass transfer rate is very low and catalyse produces only one-half of the oxygen consumed. As the reaction proceeds, the glucose concentration and the  $O_2$  uptake decrease. The mass transfer rate becomes significant and eventually equals the oxygen uptake rate, so a steady state is reached, after which the mass transfer rate exceeds the uptake rate, and the concentration of dissolved  $O_2$  increases gradually. While the oxidation kinetics of  $FADH_2$  exceeds its production rate, the predominant species will be  $FAD$  and the fluorescence intensity remains constant at the beginning. As the concentration of dissolved  $O_2$  decreases, so it does the rate of  $FAD$  regeneration. Below a given level,  $FADH_2$  becomes the predominant species and the fluorescence intensity increases. The opposite process takes place when the concentration of  $O_2$  starts to rise again by mass transfer.

The range of the maximum fluorescence intensity is *flat* enough to allows us to measure decay curves at constant intensity; thus, in silica gel we always refer to lifetime measurements carried out at the maximum intensity.

**Figure 8.** Normalized fluorescence total intensity as a function of time during the enzymatic reaction of the *GOD* entrapped in the sol gel matrix. Experimental conditions:  $\lambda_{exc} = 405$  nm,  $\lambda_{em}$  according to the passband filter described in the experimental section,  $[glucose] = 2$  mM in 0.1 M phosphate buffer,  $pH = 6.5$ .



### 3.3. Calibration Curves through Decay Curves Parameters

In Figure 9, fractional fluorescence intensities  $f_i$  of each lifetime component and the mean lifetime  $\bar{\tau}$ , retrieved from fitting with decay curves, have been reported as a function of glucose concentration.

In each panel, data exhibit a Michaelis–Menten type behaviour well described by the following expression:

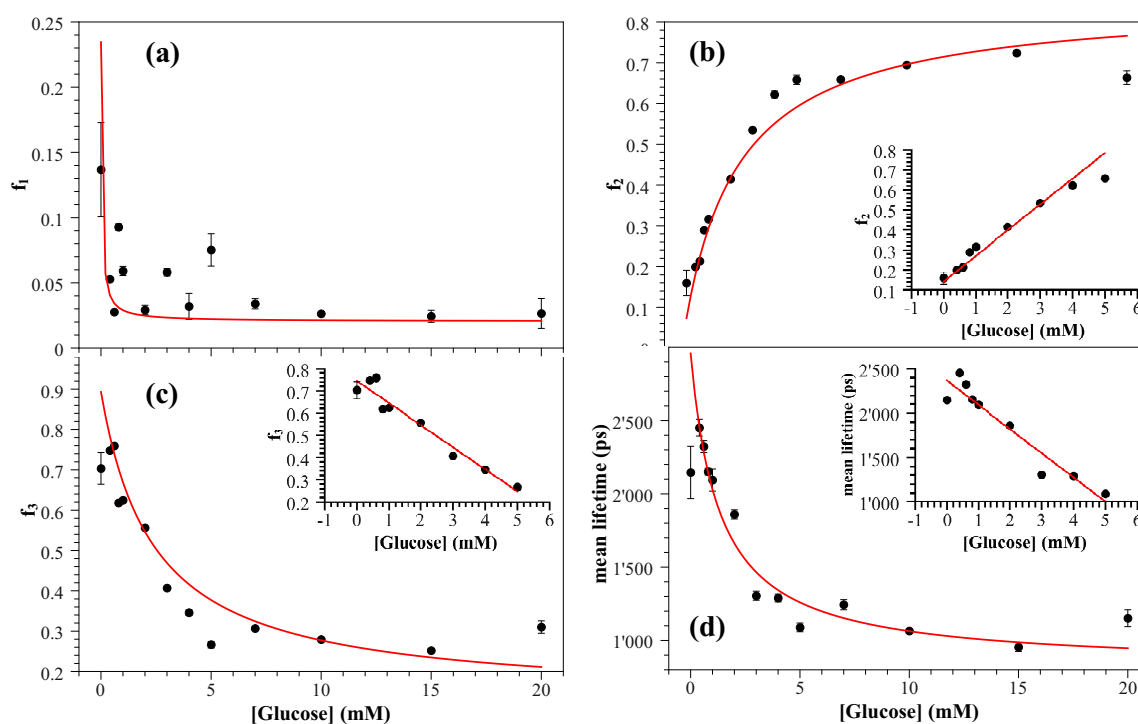
$$y = y_0 \pm \frac{y_{sat} C}{K_y + C} \quad (4)$$

where  $y$  indicates the fractional component  $f_i$  or the mean lifetime  $\bar{\tau}$ , and  $C$  is the glucose concentration. The quantity  $y_{sat}$  indicates the value at saturation and  $y_0$  is the value estimated for  $y$  when no glucose has been added ( $C = 0$ ) and  $K_y$  is a pseudo Michaelis–Menten constant. We point out that the analysis based on the Michaelis–Menten law is usually carried out by the Equation (4) without  $y_0$ , which is subtracted

from the measured  $y$  once it is estimated at  $C = 0$ . Nevertheless, since such a procedure leads to a curve forced to cross the zero, a bias in the slope may arise. Instead, we have chosen to fit our data with Equation (4) thereby considering  $y_0$  as a fitting parameter.

The sign (−) in Equation (4) has been used for fitting  $f_1$ ,  $f_3$  and  $\bar{\tau}$  (panels a, c, and d in Figure 9), whereas the sign (+) has been used for  $f_2$  (panel b in Figure 9). The decrease of the mean lifetime  $\bar{\tau}$  with the glucose concentration (panel d) can be ascribed to the dynamical fluorescence quenching of the neutral form of *FAD* caused by the excited-state isomerisation from fluorescent form to non-fluorescent form [32–34].

**Figure 9.** The fluorescence fractional components  $f_i$  retrieved from the three-exponential fitting and the mean lifetime  $\bar{\tau}$  as a function of the glucose concentration. Red curves represents the fit of data with the Michaelis–Menten like expression (4). Insets in panels b,c,d show the glucose calibration curves for each parameter.



Fitting of Equation (4) with the data reported in Figure 9 (red curves) allows us to estimate the values for  $K_y$  and  $y_{sat}$ , *i.e.*, the optokinetic parameters [31], reported in Table 2. It can be observed that the values of Michaelis–Menten constants  $K_y$  estimated from decay curves are in agreement with the ones reported in the References [23,25,31]. Particularly, the estimates retrieved from the intermediate and long fluorescence components,  $f_2$  and  $f_3$ , are very close to the values for free *GOD* measured by normalised reaction rates [25].

The inset in panels b–d of Figure 9 shows the range over which we have a linear relationship between the parameter  $y$  of the decay curves and the glucose concentration  $C$ :

$$y = S_y C + y_0 \quad (5)$$

The quantity  $S_y$  is the sensitivity of the measurement method, and the  $y_0$  is a bias term to avoid the threshold subtraction from data. Table 2 reports the best estimates of  $S_y$  from the linear fitting of

Equation (5) and the range of linearity of the calibration curves. We point out that the low temporal resolution of our detection system does not allow to resolve components with lifetime less than 30~40 ps and consequently the linear relationship between the fast fractional fluorescent component  $f_1$  and the glucose concentration cannot be investigated. Table 2 clearly shows a reduction of the linear range of about 1/4 as compared to those reported in previous work [25] where the *GOD* concentration and the thickness of the matrix were twice the values used in the present work. We wish to point out that the linear range achieved here can be easily extended as suggested in Reference [21]. The fluorescent components  $f_2$  and  $f_3$  are characterised by similar values of the sensitivity  $S_y$  which gives a limit of detection (LOD) of 0.17 mM (applying the  $S/N = 3$  criterion), whereas the LOD of the mean lifetime  $\bar{\tau}$  is 0.5 mM. Time resolved fluorescence results in a substantial improvement of the performance of the silica gel based glucose biosensor as can be seen through the comparison with the LOD value of 0.8 mM obtained by the steady state fluorescence measurements reported in Reference [25].

**Table 2.** Optokinetic parameters by Michaelis-Menten fitting of the time-resolved fluorescence parameters for the immobilized *GOD*.

|                       | $f_1$             | $f_2$                             | $f_3$                             | $\bar{\tau}$                   |
|-----------------------|-------------------|-----------------------------------|-----------------------------------|--------------------------------|
| <b>K(mM)</b>          | $0.042 \pm 0.008$ | $2.54 \pm 0.06$                   | $2.40 \pm 0.06$                   | $1.3 \pm 0.1$                  |
| $y_{\text{sat}}$      | $0.21 \pm 0.03$   | $0.781 \pm 0.002$                 | $0.764 \pm 0.001$                 | $2140 \pm 70 \text{ ps}$       |
| $S_y$                 |                   | $0.133 \pm 0.001 \text{ mM}^{-1}$ | $0.128 \pm 0.001 \text{ mM}^{-1}$ | $280 \pm 7 \text{ ps mM}^{-1}$ |
| <b>Linearity (mM)</b> |                   | 0.4–5                             | 0.4–5                             | 0.4–5                          |

The analytical performance of various *GOD* based optical biosensors is summarised in Table 3 in terms of the immobilization support, detection method, stability, linear range and detection limits. Compared to systems making use of exogenous fluorophore and exhibiting similar linear ranges [35,36], the sensing system proposed here is characterized by higher stability and slightly lower value of LOD. On the opposite our system is expected to have a lower cost in design and synthesis since it is based on the intrinsic fluorescence of *GOD*.

**Table 3.** Analytical performance of various *GOD*-based optical biosensors.

| Immobilization support          | Transducer                                  | Stability | Linearity (mM) | LoD (mM) | References |
|---------------------------------|---|-----------|----------------|----------|------------|
| PVC solid film                  | CPO fluorescence                            | 30 days   | 0.017–0.2      | 0.001    | [37]       |
| Sensing film                    | fluorescence                                | 30 days   | 0–0.5          | 0.0036   | [38]       |
| Three-layer film                | Qds and PtF <sub>2</sub> O TPP fluorescence | ?         | 0–3            | 0.2      | [35]       |
| PVA-Py matrix                   | pyrene groups fluorescence                  | 30 days   | 0.25–3         | 0.19     | [36]       |
| Silica based gels               | oxygen sensing film fluorescence            | 60 days   | 0.1–5          | 0.06     | [39]       |
| <i>GOD</i> in silica gel matrix | $f_2$ fluorescence component of <i>FAD</i>  | 60 days   | 0.4–5          | 0.17     | this paper |
| Silica gel matrix               | $f_3$ fluorescence component of <i>FAD</i>  | 60 days   | 0.4–5          | 0.17     | this paper |
| Silica gel matrix               | mean lifetime fluorescence of <i>FAD</i>    | 60 days   | 0.4–5          | 0.5      | this paper |
| Cuprophane membrane             | <i>FAD</i> fluorescence                     | ?         | 2.5–10         | ?        | [24]       |
| Silica gel matrix               | <i>FAD</i> and Tryptophan fluorescence      | 60 days   | 5–20           | 0.8      | [25]       |

#### 4. Conclusions

We have presented and described a glucose sensing system that makes use of a monolithic silica gel matrix for entrapping glucose oxidase. The dynamical changes of *FAD* fluorescence occurring during the enzymatic reaction of *GOD* with glucose have been investigated by time-resolved spectroscopy. The decay curves are well described by three-exponential model ( $\tau_1$ ,  $\tau_2$  and  $\tau_3$  being the fast, intermediate and long fluorescent lifetime, respectively) whose fractional intensities are strongly dependent on the glucose concentration. We have found that the overall enhancement of the fluorescence intensity observed after the glucose addition is due to the increase of the intermediate fluorescence component  $\tau_2$  that results from the change of the equilibrium between open and closed conformations caused by the chemical reduction of *FAD* to *FADH<sub>2</sub>*. This hypothesis is confirmed by the fluorescence quenching of the fast and long components  $\tau_1$  and  $\tau_3$ . Fluorescence quenching also indicates that the chemical reduction of *FAD* affects the photoinduced electron transfer with the surrounding aromatic residues.

Since the fractional intensities and mean lifetime are parameters strongly sensitive to the enzymatic reaction of *GOD* with glucose, they have been used to obtain calibration curves in view of possible application to biosensing. We have shown that the time resolved fluorescence can lead to LOD as low as 0.17 *mM* and provides a linear response from 0.4 *mM* to 5 *mM*. Compared to *GOD* based optical biosensor which makes use of exogenous fluorophore and have similar linear ranges, the proposed sensing system provides higher stability and slightly lower value of LOD. Moreover, it also has a lower cost in design and synthesis since it relies on the intrinsic fluorescence of *GOD*.

#### References

1. Wolfbeis, O.S. *Fluorescence Methods And Applications: Spectroscopy, Imaging, and Probes: Spectroscopy, Imaging, and Probes*; Wiley-Blackwell: Regensburg, Germany, 2008.
2. Kraayenhof, R.; Visser, A.; Gerritsen, H.; Wolfbeis, O. *Fluorescence Spectroscopy, Imaging and Probes*; Springer-Verlag: Heidelberg, Germany, 2002.
3. McShane, M.J. Potential for Glucose Monitoring with Nanoengineered Fluorescent Biosensors. *Diabet. Tech. Therap.* **2002**, *4*, 533-538.
4. Srivastava, R.; Brown, J.Q.; Zhu, H.; McShane, M.J. Stable Encapsulation of Active Enzyme by Application of Multilayer Nanofilm Coatings to Alginate Microspheres. *Macromol. Biosci.* **2005**, *5*, 717-727.
5. Brown, J.Q.; Srivastava, R.; Zhu, H.; McShane, M.J. Enzymatic Fluorescent Microsphere Glucose Sensors: Evaluation of Response Under Dynamic Conditions. *Diabet. Technol. Therap.* **2006**, *8*, 288-295.
6. Chinnayelka, S.; McShane, M.J. Glucose-Sensitive Nanoassemblies Comprising Affinity-Binding Complexes Trapped in Fuzzy Microshells. *J. Fluorescence* **2004**, *15*, 585-595.
7. Brown, J.Q.; McShane, M.J. Modeling of Spherical Fluorescent Glucose Microsensor Systems: Design of Enzymatic Smart Tattoos. *Biosens. Bioelect.* **2006**, *21*, 1760-1769.
8. Koo, Y.E.L.; Cao, Y.; Kopelman, R.; Koo, S.M.; Brasuel, M.; Philbert, M.A. Real-Time Measurements of Dissolved Oxygen Inside Live Cells by Organically Modified Silicate Fluorescent Nanosensors. *Anal. Chem.* **2004**, *76*, 2498-2505, doi: 10.1021/ac035493f.

9. Kuswandi, B.; Andres, R.; Narayanaswamy, R. Optical Fibre Biosensors Based on Immobilised Enzymes. *Analyst* **2001**, *126*, 1469-1491.
10. Foo, Y. Enzyme Kinetics: A Modern Approach. by Alejandro G. Marangoni. John Wiley & Sons, Inc.: New York, NY, USA; Hardcover, 244 pp; \$89.95; ISBN 0-471-15985-9. *Clin. Chem.* **2003**, *49*, 838, doi: 10.1373/49.5.838.
11. Cao, L.; Schmid, Rolf, D. *Carrier-Bound Immobilized Enzymes*; Wiley-VCH Verlag GmbH & Co. KGaA: Weinheim, Germany, 2005.
12. Pierre, A.C. The Sol-Gel Encapsulation of Enzymes. *Biocatal. Biotransform.* **2004**, *22*, 145-170.
13. Mac Craith, B.; Mc Donagh, C.; McEvoy, A.; Butler, T.; O'Keeffe, G.; Murphy, V. Optical Chemical Sensors Based on Sol-Gel Materials: Recent Advances and Critical Issues. *J. Sol-Gel Sci. Technol.* **1997**, *8*, 1053-1061.
14. Jin, W.; Brennan, J.D. Properties and Applications of Proteins Encapsulated within Sol-Gel Derived Materials. *Anal. Chim. Acta* **2002**, *461*, 1-36.
15. Hecht, H.J.; Kalisz, H.M.; Hendle, J.; Schmid, R.D.; Schomburg, D. Crystal Structure of Glucose Oxidase from *Aspergillus Niger* Refined at 23 Å Resolution. *J. Mol. Biol.* **1993**, *229*, 153-172.
16. Stanley, R.; MacFarlane, A. Ultrafast Excited State Dynamics of Oxidized Flavins: Direct Observations of Quenching by Purines. *J. Phys. Chem. A* **2000**, *104*, 6899-6906.
17. van den Berg, P.; Feenstra, K.; Mark, A.; Berendsen, H.; Visser, A. Dynamic Conformations of Flavin Adenine Dinucleotide: Simulated Molecular Dynamics of the Flavin Cofactor Related to the Time-Resolved Fluorescence Characteristics. *J. Phys. Chem. B* **2002**, *106*, 8858-8869.
18. Gerd, W.; Susanne, W.; Jörg, H.; Dietmar, S.; M., K.H.; Hans-Jürgen, H. A Resolution Structures of the *Penicillium Amagasakiense* and *Aspergillus Niger* Glucose Oxidases as a Basis for Modelling Substrate Complexes. *Acta Crystallograph. Sect. D* **1999**, *55*, 969-977.
19. Fujiwara, A.; Mizutani, Y. Photoinduced Electron Transfer in Glucose Oxidase: A Picosecond Time-Resolved Ultraviolet Resonance Raman Study. *J. Raman Spectroscopy* **2008**, *39*, 1600-1605.
20. Zhong, D.; Zewail, A.H. Femtosecond Dynamics of Flavoproteins: Charge Separation and Recombination in Riboflavine (Vitamin B2)-Binding Protein and in Glucose Oxidase Enzyme. *Proc. Nat. Acad. Sci. USA* **2001**, *98*, 11867-11872.
21. Sierra, J.F.; Galbàn, J.; Castillo, J.R. Determination of Glucose in Blood Based on the Intrinsic Fluorescence of Glucose Oxidase. *Anal. Chem.* **1997**, *69*, 1471-1476. doi: 10.1021/ac9611327.
22. Haouz, A.; Twist, C.; Zentz, C.; de Kersabiec, A.; Pin, S.; Alpert, B. Forster Energy Transfer from Tryptophan to Flavin in Glucose Oxidase Enzyme. *Chem. Phys. Lett.* **1998**, *294*, 197-203.
23. De Luca, P.; Lepore, M.; Portaccio, M.; Esposito, R.; Rossi, S.; Bencivenga, U.; Mita, D. Glucose Determination by Means of Steady-State and Time-Course UV Fluorescence in Free or Immobilized Glucose Oxidase. *Sensors* **2007**, *7*, 2612-2625.
24. Trettnak, W.; Wolfbeis, O.S. Fully Reversible Fibre-Optic Glucose Biosensor Based on the Intrinsic Fluorescence of Glucose Oxidase. *Anal. Chim. Acta* **1989**, *221*, 195-203.
25. Portaccio, M.; Lepore, M.; Della Ventura, B.; Stoilova, O.; Manolova, N.; Rashkov, I.; Mita, D. Fiber-Optic Glucose Biosensor Based on Glucose Oxidase Immobilised in a Silica Gel Matrix. *J. Sol-Gel Sci. Technol.* **2009**, *50*, 437-448.

26. Tolosa, L.; Malak, H.; Raob, G.; Lakowicz, J. Optical Assay for Glucose Based on the Luminescence Decay Time of the Long Wavelength Dye Cy5 (TM). *Sens. Actuat. B Chem.* **1997**, *45*, 93-99.
27. Szmactinski, H.; Lakowicz, J. Fluorescence Lifetime-Based Sensing and Imaging. *Sens. Actuat. B Chem.* **1995**, *29*, 16-24.
28. Hutchinson, C.; Lakowicz, J.; Sevickmuraca, E. Fluorescence Lifetime-Based Sensing in Tissues—A Computational Study. *Biophys. J.* **1995**, *68*, 1574-1582.
29. Bambot, S.; Rao, G.; Romauld, M.; Carter, G.; Sipior, J.; Terpetchnig, E.; Lakowicz, J. Sensing Oxygen through Skin Using a Red Diode-Laser and Fluorescence Lifetimes. *Biosens. Bioelect.* **1995**, *10*, 643-652.
30. Wolfbeis, O.S.; Oehme, I.; Papkovskaya, N.; Klimant, I. Sol-Gel Based Glucose Biosensors Employing Optical Oxygen Transducers, and a Method for Compensating for Variable Oxygen Background. *Biosens. Bioelect.* **2000**, *15*, 69-76.
31. Lepore, A.; Portaccio, M.; De Tommasi, E.; De Luca, P.; Bencivenga, U.; Maiuri, P.; Mita, D. Glucose Concentration Determination by Means of Fluorescence Emission Spectra of Soluble and Insoluble Glucose Oxidase: Some Useful Indications for Optical Fibre-Based Sensors. *J. Mol. Catal. B Enzy.* **2004**, *31*, 151-158.
32. Drossler, P.; Holzer, W.; Penzkofer, A.; Hegemann, P. Fluorescence Quenching of Riboflavin in Aqueous Solution by Methionin and Cystein. *Chem. Phys.* **2003**, *286*, 409-420.
33. Lakowicz, J.R. *Principles of Fluorescence Spectroscopy*, 2nd ed.; Kluwer Academic/Plenum: New York, NY, USA, 1999; and the bibliographical references and index therein.
34. Valeur, B. *Molecular Fluorescence: Principles and Applications*; Wiley-VCH: Weinheim, Germany, 2002; and the bibliographical references and index therein.
35. Wang, X.; Chen, H.; Zhou, T.; Lin, Z.; Zeng, J.; Xie, Z.; Chen, X.; Wong, K.; Chen, G.; Wang, X. Optical Colorimetric Sensor Strip for Direct Readout Glucose Measurement. *Biosens. Bioelect.* **2009**, *24*, 3702-3705.
36. Odaci, D.; Gacal, B.; Gacal, B.; Timur, S.; Yagci, Y. Fluorescence Sensing of Glucose Using Glucose Oxidase Modified by PVA-Pyrene Prepared via “Click” Chemistry. *Biomacromolecules* **2009**, *10*, 2928-2934.
37. Ozturk, G.; Timur, S.; Alp, S. Optical Determination of Glucose with Glucose Oxidase Immobilized in PVC together with Fluorescent Oxazol-5-One Derivatives. *Anal. Lett.* **2008**, *41*, 608-618.
38. Wang, X.; Zhou, T.; Chen, X.; Wong, K.; Wang, X. An Optical Biosensor for the Rapid Determination of Glucose in Human Serum. *Sens. Actuat. B Chem.* **2008**, *129*, 866-873.
39. Chang, G.; Tatsu, Y.; Goto, T.; Imaishi, H.; Morigaki, K. Glucose Concentration Determination Based on Silica Sol-Gel Encapsulated Glucose Oxidase Optical Biosensor Arrays. *Talanta* **2010**, *83*, 61-65.